České vysoké učení technické v Praze
Fakulta jaderná a fyzikálně inženýrská

Katedra fyziky

Studijní program: Fyzika plazmatu a termojaderné fúze

Validace rekonstrukcí magnetické rovnováhy v tokamaku pomocí simulací okrajového plazmatu transportním kódem SOLPS-ITER

Validation of tokamak equilibrium reconstructions using the SOLPS-ITER edge plasma transport code simulations

DIPLOMOVÁ PRÁCE

Vypracoval: Bc. Daniel Švorc
Vedoucí práce: Ing. Kateřina Hromasová
Konzultant: Ing. Jan Hečko
Rok: 2024

ČVUT
ČESKÉ VYSOKÉ UČENÍ TECHNICKÉ V PRAZE

ZADÁNÍ DIPLOMOVÉ PRÁCE

I. OSOBNÍ A STUDIJNÍ ÚDAJE

Příjmení: **Švorc** Jméno: **Daniel** Osobní číslo: **476658**

Fakulta/ústav: **Fakulta jaderná a fyzikálně inženýrská**

Zadávající katedra/ústav: **Katedra fyziky**

Studijní program: **Fyzika plazmatu a termojaderné fúze**

II. ÚDAJE K DIPLOMOVÉ PRÁCI

Název diplomové práce:

Validace rekonstrukcí magnetické rovnováhy v tokamaku pomocí simulací okrajového plazmatu transportním kódem SOLPS-ITER

Název diplomové práce anglicky:

Validation of tokamak magnetic equilibrium reconstructions using the SOLPS-ITER edge plasma transport code simulations

Pokyny pro vypracování:

1. Student se seznámí s tokamakem COMPASS, jeho rekonstrukcemi magnetické rovnováhy a jeho diagnostikami okrajového plazmatu.
2. Student provede několik rekonstrukcí magnetické rovnováhy ve vybraném tokamakovém výboji.
3. Student na základě těchto rekonstrukcí provede interpretativní simulace transportu v okrajovém plazmatu pomocí kódu SOLPS-ITER.
4. Student pomocí těchto simulací zvolí nejlepší variantu rekonstrukce magnetické rovnováhy.

Seznam doporučené literatury:

[1] P. C. Stangeby, The plasma boundary of magnetic fusion devices, Philadelphia Institute of Physics Publishing (2000)
[2] K. Hromasová, Interpretative SOLPS-ITER transport simulations of the COMPASS tokamak edge plasma, to be published as PhD thesis, FNSPE CTU in Prague
[3] M. Hron et al, Overview of COMPASS results, Nuclear Fusion 62.4 (2022)
[4] S. Wiesen et al, The new SOLPS-ITER code package, Journal of Nuclear Materials 463 (2015)

Jméno a pracoviště vedoucí(ho) diplomové práce:

Ing. Kateřina Hromasová katedra fyziky FJFI

Jméno a pracoviště druhé(ho) vedoucí(ho) nebo konzultanta(ky) diplomové práce:

Ing. Jan Hečko katedra fyziky FJFI

Datum zadání diplomové práce: **31.10.2023** Termín odevzdání diplomové práce: **10.05.2024**

Platnost zadání diplomové práce: **31.10.2025**

Ing. Kateřina Hromasová podpis vedoucí(ho) práce	podpis vedoucí(ho) ústavu/katedry	doc. Ing. Václav Čuba, Ph.D. podpis děkana(ky)

III. PŘEVZETÍ ZADÁNÍ

Diplomant bere na vědomí, že je povinen vypracovat diplomovou práci samostatně, bez cizí pomoci, s výjimkou poskytnutých konzultací. Seznam použité literatury, jiných pramenů a jmen konzultantů je třeba uvést v diplomové práci.

25. 3. 2024 Datum převzetí zadání	Podpis studenta

ČESKÉ VYSOKÉ UČENÍ TECHNICKÉ V PRAZE
Fakulta jaderná a fyzikálně inženýrská

Břehová 7
115 19 Praha 1

PROHLÁŠENÍ

Já, níže podepsaný

Jméno a příjmení studenta:	Daniel Švorc
Osobní číslo:	476658
Studijní program:	Fyzika plazmatu a termojaderné fúze
Studijní obor:	
Specializace:	

prohlašuji, že jsem diplomovou práci s názvem:

Validace rekonstrukcí magnetické rovnováhy v tokamaku pomocí simulací okrajového plazmatu transportním kódem SOLPS-ITER

vypracoval samostatně a uvedl veškeré použité informační zdroje v souladu s Metodickým pokynem o dodržování etických principů při přípravě vysokoškolských závěrečných prací.

Rovněž souhlasím s porovnáním textu mé kvalifikační práce s databází kvalifikačních prací Theses.cz provozovanou Národním registrem vysokoškolských kvalifikačních prací a systémem na odhalování plagiátů.

V Praze dne 10.5.2024 ..... Švorc

podpis

Poděkování

Děkuji zejména Ing. Kateřině Hromasové za profesionální vedení diplomové práce, trpělivost a ochotu. Dále bych rád poděkoval Ing. Janu Hečkovi za pomoc v důležitých chvílích. Musím také poděkovat celému COMPASS týmu za mnohá data.

Mnohokrát děkuji celé mé rodině, která mě ve studiích podporovala.

Bc. Daniel Švorc

Název práce:

Validace rekonstrukcí magnetické rovnováhy v tokamaku pomocí simulací okrajového plazmatu transportním kódem SOLPS-ITER

Autor: Bc. Daniel Švorc

Studijní program: Fyzika plazmatu a termojaderné fúze
Druh práce: Diplomová práce

Vedoucí práce: Ing. Kateřina Hromasová
Katedra fyziky, Fakulta jaderná a fyzikálně inženýrská, České vysoké učení technické v Praze
Konzultant: Ing. Jan Hečko
Katedra fyziky, Fakulta jaderná a fyzikálně inženýrská, České vysoké učení technické v Praze

Abstrakt: Přesná znalost magnetické rovnováhy tokamakového výboje je nezbytná pro řízení experimentu, analýzu dat a simulace. Rekonstrukce magnetické rovnováhy jsou však často nepřesné. Tato práce se zabývá validací pěti variant rekonstrukce rovnováhy výboje v tokamaku COMPASS #17692 pomocí transportního kódu okrajového plazmatu SOLPS-ITER. K nalezení shody mezi modelem a experimentem byla použita experimentální data. Po porovnání simulačních dat sestavených na základě různých variant rekonstrukcí rovnováhy mezi sebou a s experimentálními daty se dospělo k závěru, že použití nepřesných rekonstrukcí rovnováhy nemění konečnou shodu modelu s experimentem, pokud je lze opravit. Tímto postupem byla rovněž nalezena realističtější poloha separatrix tohoto výboje.

Klíčová slova: tokamak, rekonstrukce magnetické rovnováhy, SOLPS-ITER, plasma, simulace

Title:

Validation of tokamak equilibrium reconstructions using the SOLPS-ITER edge plasma transport code simulations

Author: Bc. Daniel Švorc

Abstract: Precise knowledge of the magnetic equilibrium of a Tokamak discharge is vital for experiment control, data analysis, and simulations. Reconstructions of the magnetic equilibrium are, however, often inaccurate. This thesis evaluates five equilibrium reconstruction variants of tokamak COMPASS discharge #17692 using SOLPS-ITER edge transport code. Experimental data were used to find a model-experiment match. After comparing the simulation data built upon different variants of equilibrium reconstructions with each other and with experimental data, it was concluded that using inaccurate equilibrium reconstructions does not change the final model-experiment match as long as they can be corrected. An optimal separatrix position for this discharge was also found using this process.

Key words: tokamak, magnetic equilibrium reconstruction, SOLPS-ITER, plasma, simulation

Contents

1 Introduction **9**
1.1 Thermonuclear fusion 10
1.2 Tokamak 10
1.3 Force equilibrium in a tokamak plasma 11
1.4 Limiter and divertor configurations 12
1.5 Scrape-Off Layer 13
1.5.1 Two-point model 14
1.6 Braginskii equations 17
1.7 SOLPS-ITER 20
1.8 COMPASS tokamak 21

2 Diagnostics **22**
2.1 Thomson scattering 23
2.2 Horizontal reciprocating probe 23
2.3 Divertor probe arrays 24
2.4 Divertor infrared camera 25
2.5 Magnetic diagnostics 26

3 Interpretative modeling with SOLPS-ITER **28**
3.1 Choosing the discharge 28
3.2 Equilibrium reconstructions 29
3.3 Validating equilibrium reconstructions based on experimental data alone 31
3.4 Matching SOLPS-ITER simulations to experimental data 32
3.5 Plasma-limiter interaction 36

Conclusion **38**

Bibliography **40**

Chapter 1

Introduction

As our planet continues to warm at an increasing rate due to the consumption of fossil fuels, we are compelled to find alternative sources of energy. One of the most ideal sources is thermonuclear fusion, where among the various concepts of achieving it, the tokamak is the most promising. It harnesses the energy of nuclear reactions in a safe and clean way. Progress in fusion research has, however, not been effortless as the construction of large experimental machines has been time-consuming and resource-intensive. Fortunately, simulations can help shed light on the processes in the tokamak.

This thesis focuses on evaluating magnetic equilibrium reconstructions of the COMPASS tokamak discharge using SOLPS-ITER code. Chapter 1 will provide an overview of the concepts, theory, and the problems involved. Chapter 2 will present diagnostics of the COMPASS tokamak used in matching the simulation to the experiment and the methods and equations used to analyze the diagnostic data. Chapter 3 is where the main work of this thesis is described. The criteria for the modeled COMPASS discharge and the discharge itself is presented. The equilibrium reconstructions along with their comparison with each other and with the diagnostic data is discussed. The reconstructions are then used as a basis for matching a SOLPS-ITER simulation to the experimental data. Based on the simulation and experimental data, the best equilibrium reconstruction is chosen.

1.1 Thermonuclear fusion

The entire field of thermonuclear fusion hinges on the existence of a reaction capable of producing energy and being achievable by our current technological means. Luckily a few of these reactions exist. The most promising is a DT reaction in which two isotopes of hydrogen, deuterium D and tritium T, fuse to create a helium nucleus, a neutron, and 17.6 MeV of energy.

$$ {}^{2}_{1}\mathrm{D} + {}^{3}_{1}\mathrm{T} \rightarrow {}^{4}_{2}\mathrm{He} + {}^{1}_{0}\mathrm{n}. \tag{1.1} $$

At temperatures achievable by current and future tokamaks of 10-20 keV, the DT reaction offers the highest cross-section (probability of the reaction occurring). The fuel is also abundant. Deuterium can be extracted from water at a low cost, while tritium can be created in a nuclear reaction of a neutron with lithium.

Tritium is an unstable isotope with a half-life of 12.3 years. As it is radioactive, it requires compliance with safety regulations. Although pure deuterium DD fuel also offers exothermic fusion reactions, they require significantly higher temperatures to achieve the necessary cross-section. DD fuel can thus be used in experimental devices not designed to reach thermonuclear conditions to test and study both the physics involved and the device itself. This way, radiation safety considerations can be alleviated by only using stable isotopes and also by having lower rate of reactions and thus lower neutron fluence.

Reaching the temperature of 10-20 keV (116-232 million degrees Celsius) is however no small feat. For comparison, the temperature in the center of the Sun is approximately 1.3 keV (15 million degrees Celsius), which is approximately 10 times lower. The fuel then needs to be kept at this temperature long enough to generate more energy than was invested for the heating and for other systems. This is the reason for needing to have a device capable of confining the fuel. [1]

1.2 Tokamak

At temperatures required for thermonuclear fusion, the DT fuel exists as a fully ionized plasma. Electrons and ions making up this plasma are electrically charged particles and in a magnetic field, they experience a Lorentz force which results in a helical trajectory along magnetic field lines. The radius of the circular component of their trajectory is called the Larmor radius. This is the basis of the tokamak, shown in figure 1.1. External coils are used to create a strong toroidal magnetic field which the particles follow. This configuration with a toroidal field only is not, however, sufficient for confining the plasma. A radial gradient and a curvature of the magnetic field is necessarily present in a toroidal configuration. The circular motion of the particles in such a field leads to drifts in a vertical direction opposite for electrons and ions. The resulting separation of charges causes an $\mathbf{E} \times \mathbf{B}$ drift and eventual loss of confinement. The $\mathbf{E} \times \mathbf{B}$ happens in a presence of an electric field and a magnetic field with the drift velocity being perpendicular to both. It is a consequence of the particles being accelerated in an electric field during their

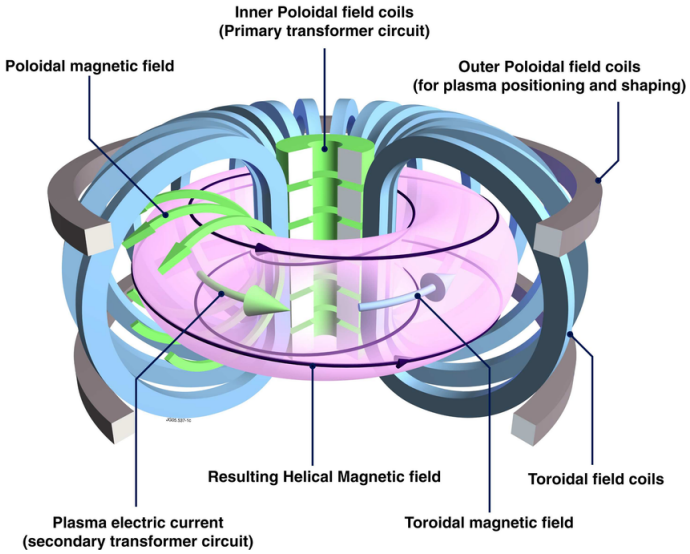

Figure 1.1: A basic scheme of a tokamak showing the magnetic field created by the plasma current and the coils. [2]

circular motion. A solution employed by tokamaks is introducing a poloidal field created by inducing a current in the plasma that flows in the toroidal direction. This combination of a toroidal and a poloidal magnetic field creates helical field lines that counteract the charge separation caused by the drifts.

1.3 Force equilibrium in a tokamak plasma

In order to achieve a steady state in a tokamak plasma discharge, a force balance must be maintained. The plasma pressure exerts an outward force and the poloidal magnetic field exerts an inward force. The imbalances between them are taken up by the magnetic pressure of the toroidal magnetic field. The toroidal geometry of the plasma leads to a force in a direction attempting to expand the plasma ring. This force is balanced by applying a vertical magnetic field which in combination with the toroidal current exerts an inward force. [1, Chapter 3]

The combined magnetic field produces an infinite set of nested toroidal magnetic surfaces. The helical magnetic field lines lie on these magnetic surfaces. As transport along magnetic field lines is high, any pressure differences are quickly removed and consequently the pressure is constant on the magnetic surfaces. To describe them, it is therefore useful to introduce a poloidal flux function ψ_p, which can be defined as $\psi_p = RA_\phi$, where R is a radial coordinate and A_ϕ is the toroidal component of magnetic vector potential. The poloidal flux is constant on the magnetic surfaces.[1]

The equilibrium between forces of the magnetic field and the plasma pressure is described by the Grad-Shafranov equation which can be written in cylindrical coordinates (R, ϕ, Z) as

$$\left(R\frac{\partial}{\partial R}\left(\frac{1}{R}\frac{\partial}{\partial R}\right)+\frac{\partial^2}{\partial Z^2}\right)\psi_p=-\mu_0 R^2\frac{\partial p}{\partial \psi_p}-\frac{1}{2}\frac{\partial\left(f^2\right)}{\partial \psi_p} \tag{1.2}$$

where p is plasma pressure, $f = RB_\phi$ and μ_0 is the vacuum permeability.[3]

In an experiment, our knowledge of the discharge and its equilibrium is limited by the available diagnostics. The Grad-Shafranov equation can therefore be used to reconstruct the equilibrium from measured data. EFIT++ [4][5] is a standard solver of the Grad-Shafranov equation designed to make such reconstructions. It parameterizes the flux functions $p' = \frac{\partial p}{\partial \psi_p}$ and $ff' = \frac{1}{2}\frac{\partial\left(f^2\right)}{\partial \psi_p}$ as polynomials or splines. Since the plasma shape influences the pressure and plasma current which in turn changes the plasma shape, an iterative scheme is used. A cost function that depends on a series of constraints coming from the diagnostic data is created. The iterative scheme then tries to minimize the cost function to find an optimal solution.

The reconstructed equilibria are, however, not always accurate. [6] This is generally tolerable for tokamak operation, such as for vertical displacement event detection and mitigation. Edge plasma studies, however, require precision in especially the separatrix position. An error in separatrix position of several centimeters has large influence on the correct determination of plasma parameters on the separatrix and in the SOL.

1.4 Limiter and divertor configurations

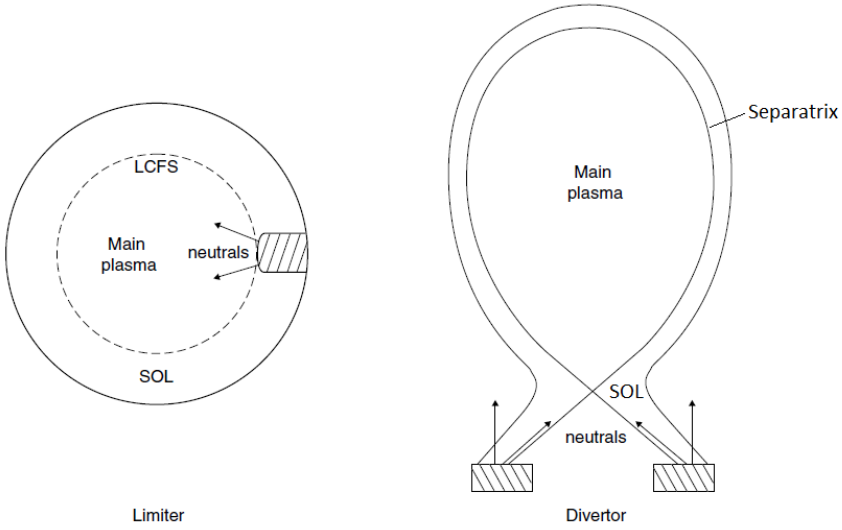

Figure 1.2: Schematics of the limiter configuration (left) and the divertor configuration (right). [7, Chapter 1]

Figure 1.2 shows two configurations of the magnetic geometry: limiter and divertor. In a tokamak, the outermost flux surface not intersecting a chamber wall is called the *last closed flux surface* or LCFS. Typically, a solid material called the *limiter*

is placed in the chamber to limit the extent of the plasma. This way, sensitive equipment within the chamber can be protected from direct contact with the plasma and plasma-wall interaction can be limited to a component designed for it. However, in this configuration the plasma is in a direct contact with the material. Particles striking the limiter can cause impurities to enter the plasma.

A *divertor* configuration is created by running electrical current in a conductor outside the plasma with the same direction as the plasma current. The magnetic field is shaped in such a way that the plasma core region is kept away from the chamber walls. An X-point is created in the magnetic field. The flux surface passing through it is called the *separatrix*, although the terms LCFS and separatrix are often used interchangeably. Particles leaving the core region are diverted by open flux surfaces onto divertor targets. Impurities released from the divertor targets are at a distance from the core region and can be swept back by the plasma flow before they can reach it. Another advantage of this configuration is that the incoming plasma can interact with the impurities and neutrals and create a temperature drop at the target. [1, Chapter 1] The following sections in this thesis will focus mainly on plasma in the divertor configuration.

1.5 Scrape-Off Layer

The LCFS or separatrix divides the tokamak plasma into two regions: the core and the *scrape-off layer* (SOL). The term scrape-off layer is used because the plasma outside the LCFS exists on open flux surfaces. After travelling a certain length along a magnetic field line, called the *connection length* L, it is scraped off by a limiter or a divertor target.

Transport in the confined plasma and the SOL is highly anisotropic. Due to the Lorentz force, plasma particles are bound to the magnetic filed lines and perpendicular (radial) transport is restricted. Experimental measurements however show much higher radial transport than values predicted by calculations from first principles. [7, Chapter 1] This increased radial transport is caused by turbulence. Most of this turbulent transport happens on the low field side (LFS) around the outer midplane. The turbulent structures are created at the LFS due to a localized interchange instability. A small radial perturbation to a boundary creates regions where grad-B and curvature drift, acting in a vertical direction, cause separation of charges. [8] This separation of charges creates an electric field which in combination with the strong toroidal field causes $\mathbf{E} \times \mathbf{B}$ drift in the radial direction. At the high field side (HFS) this drift acts in a favourable direction by stabilizing the perturbation. At the low field side the drift further amplifies the perturbation, causing instability. The instabilities grow into the so-called *blobs* and *holes*. Their movement through the edge plasma is responsible for at least 50% of the power losses from the confined plasma, constituting the major contribution of radial transport in this region. [8]

In edge plasma simulation codes, however, describing the radial transport using turbulence is too time-intensive. Instead, it is approximated with the Fick's law of

diffusion

$$\Gamma = -D_\perp \frac{\mathrm{d}n}{\mathrm{d}r}, \tag{1.3}$$

where Γ is a particle flux density and $\frac{\mathrm{d}n}{\mathrm{d}r}$ is the radial gradient of density. The cross-field transport coefficient $D_\perp$ is anomalous, refering to the dificulty of calculating it from first principles. In edge plasma transport modeling, $D_\perp$ is extracted from experimental data or scalings.

A region that plays an important role in the processes in the SOL and around the separatrix is the velocity shear layer (VSL). This layer is characterised by a large radial variation of the poloidal plasma velocity. The VSL formation is connected to the transition between open and closed magnetic field lines. In the SOL, assuming attached divertor conditions, plasma potential Φ is determined by the sheath formed at the plasma-wall boundary. The potential is equalized along the magnetic field lines by the fast parallel transport. The potential in the SOL follows the formula

$$\Phi = V_{divertor} + \alpha T_e \tag{1.4}$$

where $V_{divertor}$ is the divertor potential and $\alpha \approx 2 - 3$ in deuterium plasma. As the electron temperature T_e decreases with r in the SOL, the plasma potential Φ also decreases. In the confined plasma, the potential is determined by the radial force balance equation

$$E_r = \frac{1}{nZe}\frac{\mathrm{d}p_i}{\mathrm{d}r} - (\mathbf{u} \times \mathbf{B})_r \,, \tag{1.5}$$

where $E_r = -\frac{\mathrm{d}\Phi}{\mathrm{d}r}$ is the radial component of the electric field, Z is the ion charge, n is the plasma density, p_i is the ion pressure, $\mathbf{u}$ is the plasma velocity. If low plasma velocity $\mathbf{u}$ is assumed, the second term can be neglected. Consequently the equation shows that since the pressure decreases with increasing r, $\frac{\mathrm{d}\Phi}{\mathrm{d}r}$ is positive and therefore the plasma potential in the confined plasma increases with r. This combination with plasma potential increasing with r in the confined region and decreasing with r in the SOL creates a peak in the transition area. The radial electric field $E_r = -\frac{\mathrm{d}\Phi}{\mathrm{d}r}$ in combination with the toroidal magnetic field gives rise to an $\mathbf{E} \times \mathbf{B}$ drift velocity in the poloidal direction. This variation in poloidal velocity constitutes the VSL. Although this explanation is heavily simplified and does not take into account other important effects such as turbulence, the VSL has been observed across many tokamak experiments and simulations. [9][6] The VSL and its potential maximum is used in this thesis as an indication of the separatrix position.

1.5.1 Two-point model

One of the main advantages of the divertor configuration is the possibility of creating a temperature gradient along the SOL. This allows the coexistence of a hot upstream plasma compatible with high fusion power, and cold divertor target plasma, compatible with long divertor lifetime. The two-point model simplifies the SOL into two points: the *upstream* halfway between the targets (where most of the plasma heat enters SOL) and *downstream* at divertor targets. A diagram of the two-point model can be seen on figure 1.3. The two-point model works under the following assumptions.

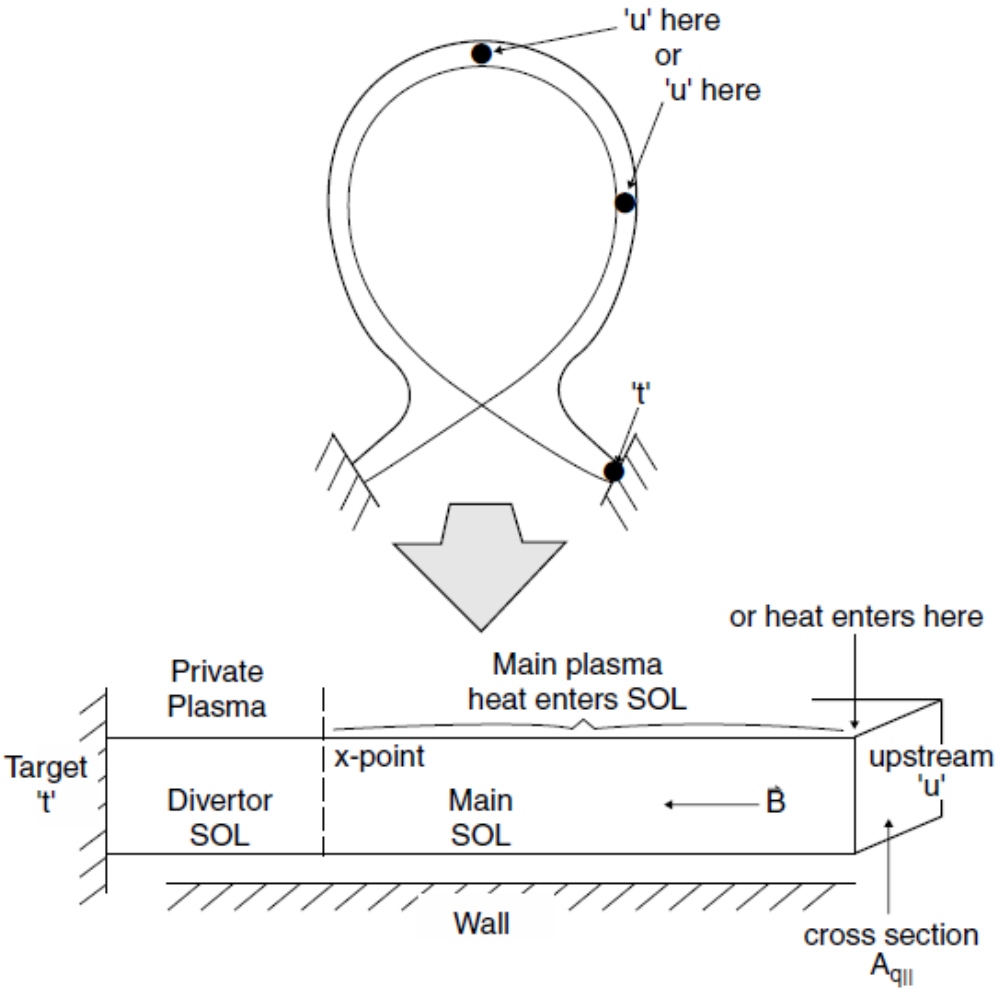

Figure 1.3: The simplified scrape-off layer used in the two-point model. The precise location of the 'upstream' location is not critical. [7, Chapter 5]

1. *Particle balance.* The recycled neutrals from the targets are all ionized in a thin layer near the target. Additionally, a neutral which resulted from an ion impacting the target while travelling along a particular magnetic field line is assumed to be re-ionized on the same field line. Each magnetic field line has therefore its own localized particle balance. This means that particles along a certain field line spend part of their time as ions and part of their time as neutrals. There is no parallel flow in most of the SOL except above the target where it increases from zero in the ionization layer to a sheath entrance speed which is taken as the sound speed

$$c_s = \sqrt{\frac{e\,(T_i + T_e)}{m_i + m_e}}. \tag{1.6}$$

2. *Pressure balance.* Friction between the thin ionization region and the target and viscous effects are disregarded. Total pressure along each of the SOL mag-

netic field lines is then constant

$$p + nmv^2 = constant. \tag{1.7}$$

With additional assumption of equal ion and electron temperature $T_e = T_i$ it is possible to write the static part of the total pressure as

$$p = neT_e + neT_i = 2neT. \tag{1.8}$$

The dynamic part is $p_{dyn} = mnv^2$. Flow velocity is zero in most of the upstream region up to the ionization layer. The velocity at the target is taken as the sound speed. Combining the equations it is possible to write the pressure balance between the upstream (u) and target (t) as

$$2n_tT_t = n_uT_u \tag{1.9}$$

3. *Power balance.* Parallel energy flux is carried solely by conduction since flow velocity is zero in most of the SOL. Assuming that parallel heat flux density $q_{||}$ enters the SOL upstream and is removed at the target at a length L without any losses then it is possible to write

$$T_u^{7/2} = T_t^{7/2} + \frac{7}{2}q_{||}\frac{L}{\kappa_{0e}}. \tag{1.10}$$

$\kappa_{0e} = 2000$ is the electron parallel conductivity coefficient while ion conductivity is neglected as it is negligible in comparison. Assuming temperature drop across the ionization layer is zero (it is assumed to be a thin layer) the equation for how much power density is exhausted through the sheath is

$$q_{||} = \gamma n_t e T_t c_{st}, \tag{1.11}$$

where γ is the sheath heat transmission coefficient, $\gamma \approx 7$.

The final set of equations for the two-point model (2PM) is then [7]

$$2n_tT_t = n_uT_u \tag{1.12}$$

$$T_u^{7/2} = T_t^{7/2} + \frac{7}{2}q_{||}\frac{L}{\kappa_{0e}} \tag{1.13}$$

$$q_{||} = \gamma n_t e T_t c_{st} \tag{1.14}$$

The two-point model is a useful tool for approximating SOL behavior in plasma modeling. It can also be used to approximate position of the separatrix by relating divertor measurements with upstream measurements. Equation (1.13) provides a relationship between the strike point temperature and the upstream separatrix temperature.

1.6 Braginskii equations

One approach in describing plasma behavior is using the *fluid equations*. Their derivation follows from the kinetic equation

$$\frac{\partial f_a}{\partial t} + \frac{\partial f_a}{\partial x_k}\frac{\mathrm{d}x_k}{\mathrm{d}t} + \frac{\partial f_a}{\partial v_{k,a}}\frac{\mathrm{d}v_{k,a}}{\mathrm{d}t} = \left(\frac{\partial f_a}{\partial t}\right)_{coll}. \tag{1.15}$$

This equation describes a time evolution of a distribution function $f(\mathbf{x}, \mathbf{v}, t)$ of particle species a. Its variables are: time t, position $\mathbf{x}$ and velocity $\mathbf{v}$. The term on the right-hand side of the equation $\left(\frac{\partial f_a}{\partial t}\right)_{coll}$ represents changes in the distribution function due to binary collisions between particles of the same species or with other species. The distribution function is normalized in such a way that an integral over a region in spatial position $\mathbf{x}$ and velocity position $\mathbf{v}$ gives the number of particles of a given species in that region, i.e,

$$\int f_a(\mathbf{x}, \mathbf{v}, t)\mathrm{d}^3\mathbf{x}\mathrm{d}^3\mathbf{v} = N_a(t). \tag{1.16}$$

One can calculate *moments* by multiplying the kinetic equation by powers of $\mathbf{v}$ and integrating over that variable. These powers can represent different physical quantities such as number of particles $\mathbf{v}^0 = 1$, momentum $m\mathbf{v}$, kinetic energy $\frac{1}{2}m\mathbf{v}^2$, etc. The resulting equations then represent conservation laws of the quantities. By calculating moments for higher and higher powers one would obtain an infinite set of equations that would be equivalent to the kinetic equation. To obtain the fluid equations however, only the first three moments are used with the rest being replaced by different formulas based on additional assumptions. This is called a *closure*. [10] There are many types of closures for fluid equations such as the Braginskii, Balescu or Zhdanov closure. [11][12][13] This thesis will present assumptions and fluid equations of the Braginskii closure.

The underlying idea of the closure is that the distribution function can be expanded about a Maxwellian distribution, i.e.,

$$f = f_0 + \delta f \tag{1.17}$$

with

$$f_0 = \frac{n_a}{\left(2\pi T_a/m_a\right)^{3/2}} \exp\left(-\frac{m_a}{2T_a}\left(\mathbf{v}' - \mathbf{w}\right)^2\right) \tag{1.18}$$

where $\mathbf{v}'$ is the velocity coordinate and $\mathbf{w}$ is the mean velocity. By solving the kinetic equation with small gradients and drift velocities it is possible to get formulas for collisional drag, viscosity and thermal conduction. The formulas can then be used as a closure for fluid equations. The formulas are derived under the following assumptions

- The mean free path is short compared to macroscopic lengths.
- The plasma consists of electrons and singly charged ions.

- The plasma is quasineutral, i.e., $n_e = n_i = n$.
- The plasma evolves at much larger time scales than the typical collision time.

The Braginskii fluid equations are then the following. The *continuity equation* for species a, electrons or ions, is

$$\frac{\mathrm{d}n_a}{\mathrm{d}t} = -n_a \nabla \cdot \mathbf{v}_a \tag{1.19}$$

where the total derivative is

$$\frac{\mathrm{d}}{\mathrm{d}t} = \frac{\partial}{\partial t} + \mathbf{v}_a \cdot \nabla. \tag{1.20}$$

The *momentum balance* equation is

$$n_a m_a \frac{\mathrm{d}\mathbf{v}_a}{\mathrm{d}t} = -\nabla p_a - \frac{\partial}{\partial x_\beta}\Pi_{a\alpha\beta} + n_a e_a \left(\mathbf{E} + \mathbf{v}_a \times \mathbf{B}\right) + \mathbf{R}_a \tag{1.21}$$

where $p_a = n_a T_a$ and repeated Greek indices imply summation. $\mathbf{R}_j$ is the rate of momentum transfer due to collisions. There are only two species and so $\mathbf{R}_i = -\mathbf{R}_e$. The rate of momentum transfer from ions to electrons is caused by the friction force $\mathbf{R}_u$ and the thermal force $\mathbf{R}_T$

$$\mathbf{R}_e = \mathbf{R}_u + \mathbf{R}_T. \tag{1.22}$$

The friction force is

$$\mathbf{R}_u = -\frac{m_e n}{\tau_e}(0.51 u_{||} + u_\perp) = ne(\eta_{||} j_{||} + \eta_\perp j_\perp) \tag{1.23}$$

where $u = v_e - v_i$, η is the electrical resistivity, j is the plasma current and the subscripts $||$ and $\perp$ are parallel and perpendicular directions to the magnetic field.

The thermal force is

$$\mathbf{R}_T = -0.71 n \nabla_{||} T_e - \frac{3}{2}\frac{n}{|\omega_{ce}|\tau_e}\mathbf{b} \times \nabla T_e \tag{1.24}$$

where $\mathbf{b}$ is a unit vector parallel to the magnetic field.

The stress tensors for electrons and ions both have the same form differing only in the viscosity coefficients η. In $[x, y, z]$ Cartesian coordinate system where z-axis is parallel to the magnetic field it is

$$\begin{aligned}
\Pi_{zz} &= -\eta_0 W_{zz} \\
\Pi_{xx} &= -\frac{1}{2}\eta_0(W_{xx} + W_{yy}) - \frac{1}{2}\eta_1(W_{xx} - W_{yy}) - \eta_3 W_{xy} \\
\Pi_{yy} &= -\frac{1}{2}\eta_0(W_{xx} + W_{yy}) - \frac{1}{2}\eta_1(W_{yy} - W_x) + \eta_3 W_{xy} \\
\Pi_{xy} &= \Pi_{yx} = -\eta_1 W_{xy} + \frac{1}{2}\eta_3(W_{xx} - W_{yy}) \\
\Pi_{xz} &= \Pi_{zx} = -\eta_2 W_{xz} - \eta_4 W_{yz} \\
\Pi_{yz} &= \Pi_{zy} = -\eta_2 W_{yz} + \eta_4 W_{xZ}
\end{aligned} \tag{1.25}$$

$W_{\alpha\beta}$ is the rate-of-strain tensor

$$W_{\alpha\beta} = \frac{\partial v_\alpha}{\partial x_\beta} + \frac{\partial v_\beta}{\partial x_\alpha} - \frac{2}{3}\delta_{\alpha\beta}\nabla\cdot\mathbf{v}. \tag{1.26}$$

where δ is the Kronecker delta. The ion viscosity coefficients are

$$\begin{aligned} \eta_0^i &= 0.96 n_i T_i \tau_i \\ \eta_1^i &= \frac{3}{10}\frac{n_i T_i}{\omega_{ci}^2\tau_i} \qquad \eta_2^i = 4\eta_1^i \\ \eta_3^i &= \frac{1}{2}\frac{n_i T_i}{\omega_{ci}} \qquad \eta_4^i = 2\eta_3^i \end{aligned} \tag{1.27}$$

and the electron viscosity coefficients are

$$\begin{aligned} \eta_0^e &= 0.73 n_e T_e \tau_e \\ \eta_1^e &= 0.51\frac{n_e T_e}{\omega_{ce}^2\tau_e} \qquad \eta_2^e = 4\eta_1^e \\ \eta_3^e &= -\frac{1}{2}\frac{n_e T_e}{|\omega_{ce}|} \qquad \eta_4^e = 2\eta_3^e. \end{aligned} \tag{1.28}$$

Where $\omega_{ci} = \frac{eB}{m_i}$ and $\omega_{ce} = \frac{eB}{m_e}$ are the ion and electron cyclotron frequencies. The ion and electron collision times are

$$\begin{aligned} \tau_i &= 12\pi^{3/2}\frac{\varepsilon_0^2 m_i^{1/2} T_i^{3/2}}{n e^4 \ln\Lambda} \\ \tau_e &= 3(2\pi)^{3/2}\frac{\varepsilon_0^2 m_e^{1/2} T_e^{3/2}}{n e^4 \ln\Lambda} \end{aligned} \tag{1.29}$$

where $\ln\Lambda$ is the Coulomb logarithm and ε_0 is the vacuum permittivity.

The *energy balance* equation is

$$\frac{3}{2}n\frac{\mathrm{d}T_a}{\mathrm{d}t} = -p_a\nabla\cdot\mathbf{v}_a - \nabla\cdot\mathbf{q}_a - \Pi_{a\alpha\beta}\frac{\partial v_{a\alpha}}{\partial x_\beta} + Q_a. \tag{1.30}$$

Like the rate of momentum transfer, the electron energy flux density is made up of two contributions: friction and thermal energy flux density $\mathbf{q}^e = \mathbf{q}_u^e + \mathbf{q}_T^e$. The energy flux density due to friction is

$$\mathbf{q}_u^e = nT_e\left(0.71\mathbf{u}_{||} + \frac{3/2}{|\omega_{ce}|\tau_e}\mathbf{b}\times\mathbf{u}\right) \tag{1.31}$$

and the thermal energy flux density is

$$\mathbf{q}_T^e = \frac{nT_e\tau_e}{m_e}\left(-3.16\nabla_{||}T_e - \frac{4.66}{\omega_{ce}^2\tau_e^2}\nabla_\perp T_e - \frac{5/2}{|\omega_{ce}|\tau_e}\mathbf{b}\times\nabla T_e\right). \tag{1.32}$$

The ion energy flux density is

$$\mathbf{q}_i = \frac{nT_i\tau_i}{m_i}\left(-3.9\nabla_{||}T_i - \frac{2}{\omega_{ci}^2\tau_i^2}\nabla_\perp T_i - \frac{5/2}{|\omega_{ci}|\tau_i}\mathbf{b}\times\nabla T_i\right). \tag{1.33}$$

The heat exchange between ions and electrons due to collisions gives rise to the ion heating

$$Q_i = \frac{3m_e}{m_i}\frac{n}{\tau_e}(T_e - T_i) \tag{1.34}$$

and the electron heating is

$$Q_e = \eta_{||} j_{||}^2 \eta_\perp j_\perp^2 + \frac{1}{ne}\mathbf{j}\cdot\mathbf{R}_T + \frac{3m_e}{m_i}\frac{n}{\tau_e}(T_i - T_e). \tag{1.35}$$

1.7 SOLPS-ITER

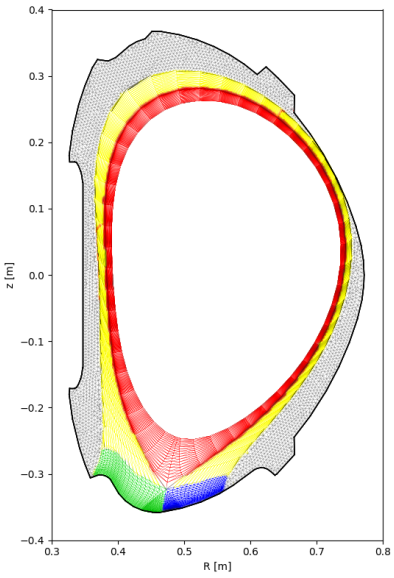

Figure 1.4: The B2.5 mesh is separated into four regions: core (red), SOL (yellow), inner divertor (green) and outer divertor (blue).

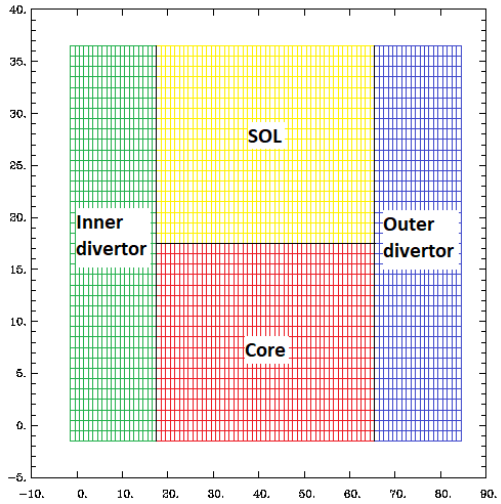

Figure 1.5: Unwrapped representation of the B2.5 mesh.

SOLPS-ITER is a tokamak boundary plasma code package developed over the years by various research groups and more recently by the ITER Organization. At its core it is a combination of two codes: B2.5, which is a 2D multi-fluid plasma transport code, and EIRENE, which handles neutral particles using a 3D kinetic Monte Carlo approach. It is the Braginskii equations which are used by B2 for the fluid simulation. SOLPS-ITER uses the toroidal symmetry of the tokamak to simplify the simulation into a 2D poloidal cross-section.[14]

The plasma around the separatrix is separated into regions. This allows the mesh to be displayed on a straightened 2D surface, figure 1.4. The quadrangular mesh belongs to B2.5. It is aligned to magnetic surfaces in such a way that when it is straightened out (figure 1.5), its principal two directions correspond to the radial transport and the parallel transport. This allows for decoupling the radial and parallel transport in the simulation. The regions are separated by boundaries for which boundary conditions can be set. The SOLPS-ITER code package includes a program `DivGeo`

used to construct the simulation geometry. Programs `carre` and `triang` are used to construct the B2 and EIRENE mesh. Importantly, a magnetic equilibrium serves as a basis for constructing the mesh. [15]

1.8 COMPASS tokamak

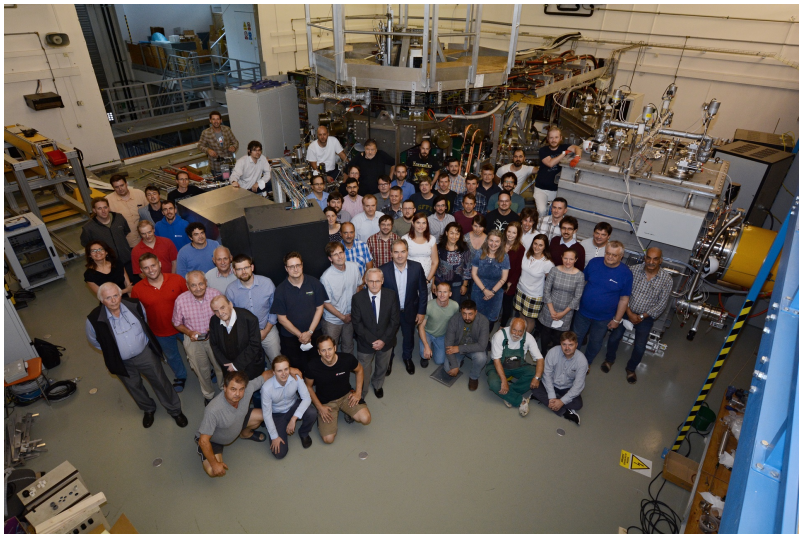

Figure 1.6: The COMPASS tokamak and team.

COMPASS was an experimental tokamak that was operated by the Institute of Plasma Physics of the Czech Academy of Sciences between 2009 and 2021, see figure 1.6. It had a major radius of $R = 0.56$ m, minor radius $a = 0.23$ m, toroidal magnetic field $B_T = 0.9 - 1.7$ T, plasma current I_p up to 350 kA and pulse duration <500 ms. It was possible to operate it in a lower single-null divertor configuration and in inner wall limited configuration. The plasma shape in COMPASS was similar to the ITER tokamak at one tenth scale. This made it possible to study physics relevant to ITER. [16][17]

During its operation, several methods of magnetic reconstructions were used and developed. These are further elaborated in section 3.2. It has been shown that reconstructed separatrix position may be inaccurate. [6] Additionally, the different methods of magnetic reconstructions can give different results.

This can have significant impact on SOLPS-ITER as it uses a magnetic reconstruction as a basis for its computational grid. [18] The aim of this thesis is to evaluate the magnetic reconstructions on a given COMPASS discharge by using them as a basis for SOLPS-ITER simulations. Diagnostic data are used to fine-tune the simulations to achieve the best experiment-model match. The best magnetic reconstruction is then proposed.

Chapter 2

Diagnostics

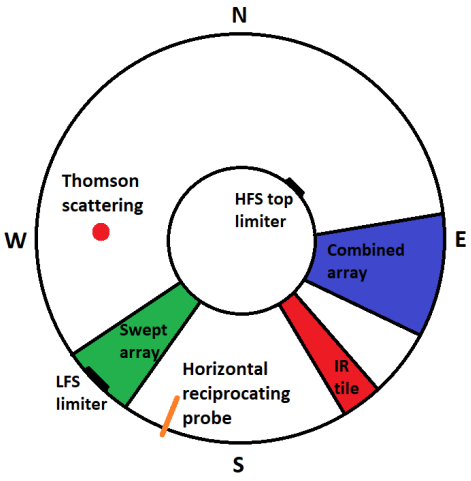

Figure 2.1: Toroidal view of the COMPASS tokamak showing the location of its diagnostics.

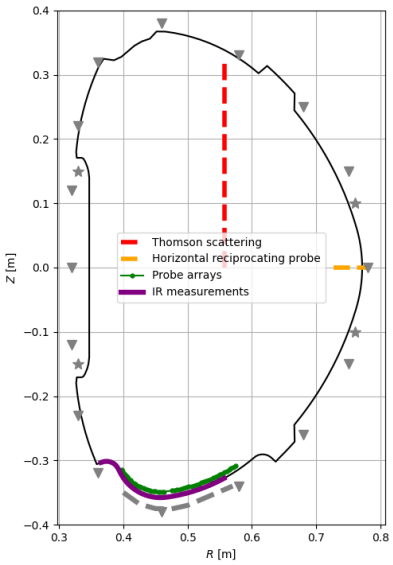

Figure 2.2: Poloidal cross-section of the COMPASS tokamak and the location of its diagnostics.

This chapter will introduce the diagnostics of tokamak COMPASS used in interpretative SOLPS-ITER simulations. Two diagnostics offer upstream measurements in two different poloidal positions: the Thomson scattering diagnostic and the horizontal reciprocating probe. Downstream measurements are provided by the two divertor probe arrays and the infrared (IR) camera. Magnetic diagnostics provide data for equilibrium reconstructions and a visible spectrum camera is used to gauge the interaction of SOL plasma with limiters. The diagnostics are shown in figures 2.1, 2.2 in a toroidal location (left) and poloidal location (right).

2.1 Thomson scattering

The Thomson scattering diagnostic provides measurement of electron temperature T_e and electron density n_e. A laser pulse is shot in the plasma. Photons scattered on electrons in plasma due to the physical process of Thomson scattering are collected by viewing optics directed at the laser path. The scattered photons undergo a frequency shift that depends on the velocity of the scattering electrons. Spectrum of the collected light then carries information about the electron velocity distribution and thus their temperature T_e. Additionally, intensity of the scattered light provides information about electron density n_e.

In tokamak COMPASS, the laser systems consisted of four Nd:YAG lasers each capable of 30 Hz repetition rate. All lasers were fired in a vertical direction at top of the tokamak with mutual separation of 3 mm. They were fired alternately, thus achieving 120 Hz repetition rate. Two objective lenses that were directed at the plasma core and at the edge region were used to collect the scattered light from 56 spatial points. The light was led into polychromators which was used to resolve the spectrum. [19] [20]

2.2 Horizontal reciprocating probe

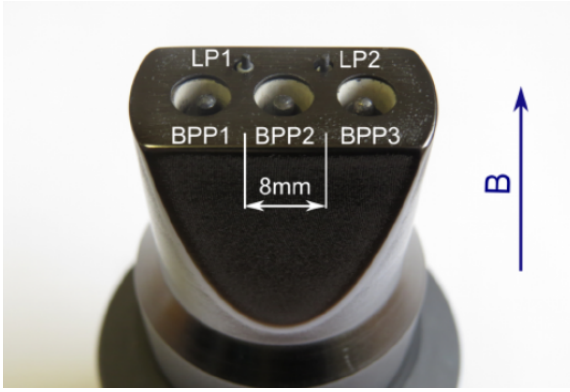

Figure 2.3: The probe head used by the horizontal reciprocating probe. It carries two Langmuir probes (LP) and three ball-pen probes. [21]

The COMPASS tokamak featured a reciprocating manipulator that was used to insert a probe head carrying a combination of Langmuir probes (LP) and ball-pen probes (BPP) into the plasma. The horizontal reciprocating probe (HRCP) was installed at the outer midplane and entered the plasma horizontally. By fast movement in and out of the plasma ($\sim$ 0.1 s), a spatial profile of plasma parameters was measured. On COMPASS discharge #17692 (discussed further in this thesis), the installed probe head carried two Langmuir probes, one electrically floating and one collecting the ion saturation current, and three floating ball-pen probes (Fig. 2.3). This configuration allows for the measurement or determination of various quantities, such as probe floating potential, probe ion saturation current, electron temperature, electron density, plasma potential and heat flux.

The electron temperature can be determined from a pair of one floating Langmuir probe and one floating ball-pen probe. The Langmuir probe collecting charged particles creates a floating potential

$$V_{LP,fl} = \Phi - 2.8T_e \tag{2.1}$$

where Φ is the plasma potential. The floating potential of a ball-pen probe is

$$V_{BPP,fl} = \Phi - 0.6T_e. \tag{2.2}$$

Electron temperature can thus be determined by subtracting the equations (2.1) and (2.2) as

$$T_e = \frac{V_{BPP,fl} - V_{LP,fl}}{2.2}. \tag{2.3}$$

The one remaining Langmuir probe collected the ion saturation current by being biased with constant negative voltage to repel all electrons. The ion saturation current collected by the probe is then

$$I_{sat} = \frac{1}{2} e A n_e c_s \tag{2.4}$$

where A is the probe collecting area.[7, Chapter 2] From this measurement an electron density can be then deduced since the sound speed c_s can be calculated using (1.6). [21]

2.3 Divertor probe arrays

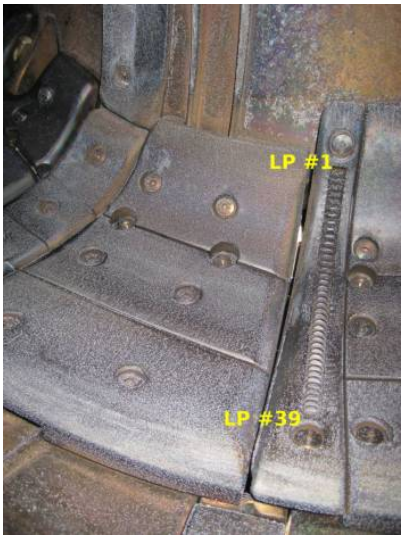

Figure 2.4: The swept probe array made up of 39 Langmuir probes (LP).[22]

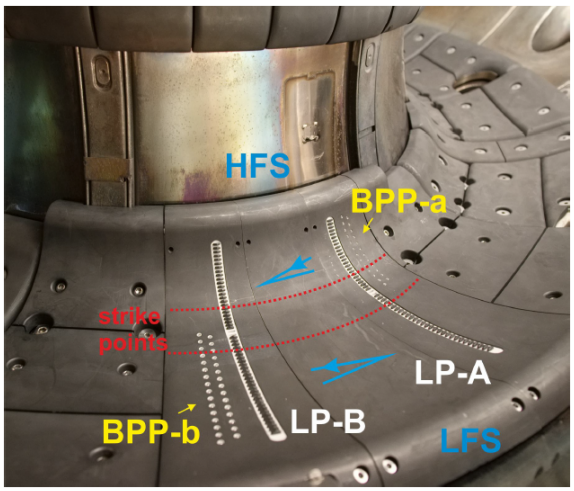

Figure 2.5: The combined probe array. It uses a combination of 55 Langmuir probes (LP) and 56 ball-pen probes (BPP). [23]

Two divertor probe arrays were installed at the tokamak COMPASS: the *combined probe array* and the *swept array*. Arrays are shown in figures 2.5, 2.4.

The combined array is made up of two full arrays of 55 Langmuir probes and one array of 56 ball-pen probes. Their measurements are combined to gauge plasma parameters, thus the "combined" probe array. The measurement uses the same principle as on the reciprocating probe head. Probes biased with a large negative voltage measure the ion saturation current while probes in the floating mode measure the floating potential. The combination of Langmuir probes and ball-pen probes then provide information about the electron temperature, electron density and parallel heat flux.

The combined divertor probe arrays uses a different design of Langmuir probes and thus the formula for their floating potential is different [23]

$$V_{LP,fl} = \Phi - 2.0T_e. \tag{2.5}$$

The floating potential of the ball-pen probes is the same as for the reciprocating probes, equation (2.2). Electron temperature can be thus calculated as

$$T_e = \frac{V_{BPP,fl} - V_{LP,fl}}{1.4}. \tag{2.6}$$

The divertor heat flux parallel to the field lines is calculated as

$$q_{||} = \frac{I_{sat}}{A}\left(2.5T_e + V_{fl,BPP} + 2T_e \min(7, e^{-V_{fl,LP}/T_e}) + 14.6 \text{ eV}\right) \tag{2.7}$$

with I_{sat} being calculated similarly to equation (2.4) using $A = 2.8$ mm^2.[24]

The swept probe array consists of 39 Langmuir probes that can be biased to collect the ion saturation current, electrically floating or swept to register the I-V characteristic. On COMPASS discharge #17692 the array was operated in the swept mode, which is why it is referred to as the swept array in this thesis. Various methods can be utilized to extract plasma parameters from the I-V curve such as a three or four-parameter fit. [25] The quantities extracted include the electron temperature T_e, electron density n_e, ion saturation current I_{sat}, parallel heat flux $q_{||}$ and others. The data from the swept array from discharge #17692 was analyzed using the three-parameter fit.

2.4 Divertor infrared camera

The COMPASS tokamak was equipped with several infrared (IR) cameras, one of which was directed at the divertor region. A special graphite divertor tile optimized for IR thermography was used. The tile was attached with a special rail system which provided precise alignment necessary for proper extraction of the parallel heat flux. Knowledge of thermal conduction from and within the tile and a precise calibration using an embedded heating element allowed for a precise determination of the temperature of the tile. The camera offered measurements with high spatial and temporal resolution. [26]

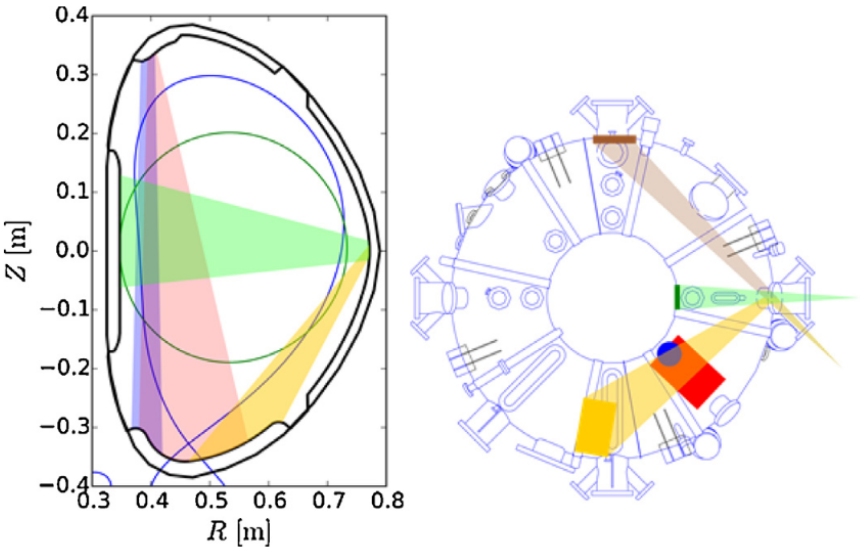

Figure 2.6: Poloidal and toroidal location and field-of-view of five infrared cameras at COMPASS. The divertor infrared camera is plotted in red. [26]

2.5 Magnetic diagnostics

The COMPASS tokamak was equipped with large amount of magnetic diagnostics. About 440 coils of various types were positioned all over the vacuum vessel. They allowed for measurements of various quantities such as plasma current I_p, loop voltage U_{loop}. The set of coils most relevant to this thesis is, however, the set of 16 inner partial Rogowski coils for measurements of B_θ, installed in 16 poloidal positions around the plasma at one toroidal angle. Their measurements were used as input constraints for standard magnetic equilibrium reconstructions, together with measurements of the toroidal magnetic field, plasma current, current in the poloidal field coils and chamber geometry. [20] An additional set of Mirnov coils comprised of 8 tangential and 8 normal coils was positioned in divertor region. Together with 4 flux loops directly measuring poloidal flux they can be used as additional constraints for equilibrium reconstructions. [27]

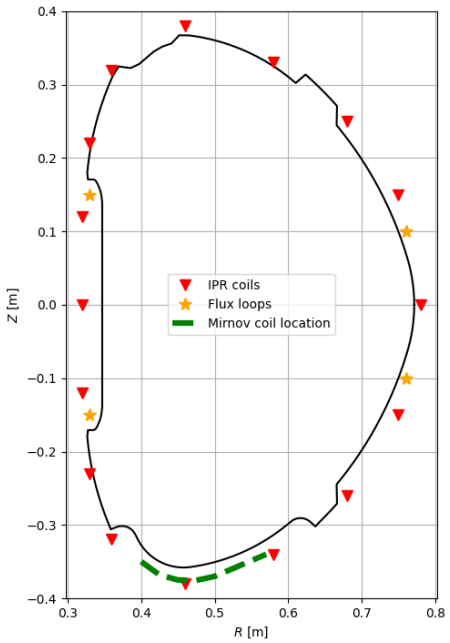

Figure 2.7: Poloidal location of the inner partial Rogowski coils (red), flux loops (orange) and Mirnov coils (green).

Chapter 3

Interpretative modeling with SOLPS-ITER

This chapter first describes the COMPASS discharge used in this thesis, then its diagnostic measurements are compared with equilibrium reconstruction variants, which are then used for SOLPS-ITER simulations. Finally, the simulation results are discussed and used to infer information about the separatrix position and the accuracy of the equilibrium reconstructions.

3.1 Choosing the discharge

The first step of this thesis was choosing the tokamak discharge to be modeled. During operation of the COMPASS tokamak, over twenty thousand discharges were carried out. The discharge selected must accurately reflect a typical mode of operation while avoiding characteristics that might hinder comparisons between simulations utilizing different equilibrium reconstructions and characteristics that could compromise the accuracy of simulations using SOLPS-ITER, such as experiments with impurity gas puffs, resonant magnetic perturbations or strong runaway electron beams. The focus of this thesis is on comparison of magnetic equilibrium reconstructions. The most apparent difference between various magnetic equilibrium reconstructions is the position of the separatrix. For this reason, another requirement for the chosen discharge was a good coverage by diagnostics measuring the separatrix position and diagnostics facilitating interpretative modeling with SOLPS-ITER. The last criterion was a reasonably stationary profile of plasma parameters to select the time instance to be modeled.

The discharge to be modeled, selected with K. Hromasová, is the COMPASS discharge #17692. It is an L-mode discharge in a lower single-null divertor configuration. The toroidal magnetic field was $B_t = -1.38$ T, the plasma current was $I_p = 200$ kA. The Thomson scattering diagnostic shows core density $n_e = 4.5 \times 10^{19}$ m^{-3}. Upstream measurements in the selected discharge are provided by the Thomson scattering diagnostic at the top of the plasma and the horizontal reciprocating probe at the outer midplane. The divertor is well covered by diagnostic measurements of the

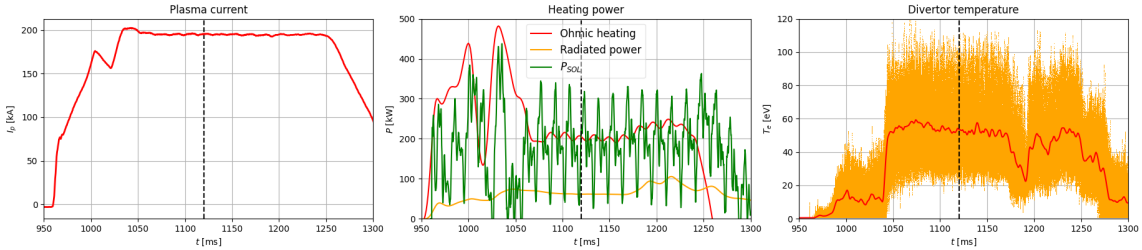

Figure 3.1: Time evolution of the plasma current, heating power and divertor electron temperature. The simulated time 1120 ms is marked by the vertical line.

combined probe array, swept probe array and the infrared camera. Field of view of the IR camera captured both divertor plates and the strike points.

The modeled time was chosen to be 1120 ms. Figure 3.1 shows time evolution of plasma parameters with the time highlighted. As the horizontal reciprocating probe can disturb the plasma and affect measurements from other diagnostics, the modeled time instance is before the probe penetrated deep into the plasma at 1170 ms.

3.2 Equilibrium reconstructions

This thesis uses and evaluates five different methods of magnetic equilibrium reconstructions that were used and developed during the operation of the COMPASS tokamak. These methods use diagnostic measurements and results from various models as inputs to the EFIT++ Grad-Shafranov equation solver. The first, so-called *standard* equilibrium reconstruction uses B_θ measurements from the 16 Inner Partial Rogowski (IPR) coils (figure 2.7) as an important constraining input. Other inputs include toroidal magnetic field, plasma current and geometry of the first wall.

Precise information of the IPR coils position and angle is crucial for accurate equilibrium reconstructions. It has been shown that the recorded values may be inaccurate. A study by O. Kovanda used IPR coils position and angles variations of EFIT++ input of a vacuum discharge #6413 to find the most likely corrections. These corrections can be used to improve equilibrium reconstructions in other discharges. [27] A systematic study of COMPASS discharges with recorded VSL position by reciprocating probes has shown that these corrections reduce the difference between measured VSL position and reconstructed separatrix position. [6] Additionally, four flux loops (FL) and two sets of divertor Mirnov coils (MC) can be used to further improve the reconstructions by providing additional magnetic measurements.[27]

Another refinement to the standard equilibrium reconstruction uses Thomson scattering measurements to provide a realistic pressure radial profile as input to EFIT++. To provide total plasma pressure to the algorithm, the ion pressure profile is assumed to be the same as the electron pressure, $p = 2p_e$.

The final method of improving the standard equilibrium reconstruction uses the two-point model. Upstream temperature on the separatrix can be calculated using equation (1.13). The upstream temperature is then compared to the Thomson scat-

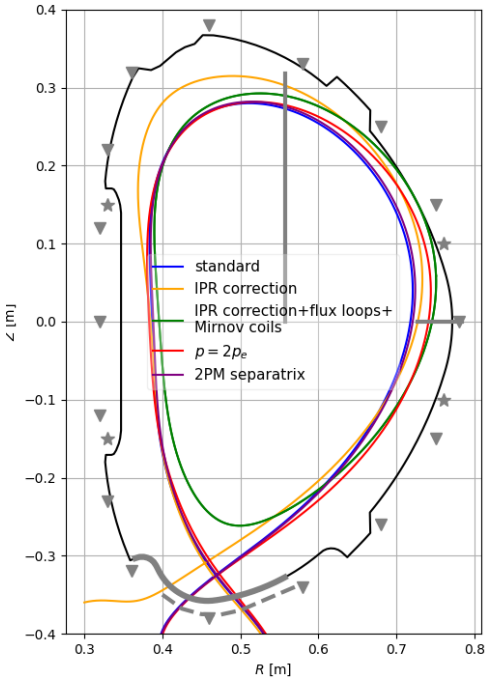

Figure 3.2: Comparison of the separatrix position between the five equilibrium reconstruction variants.

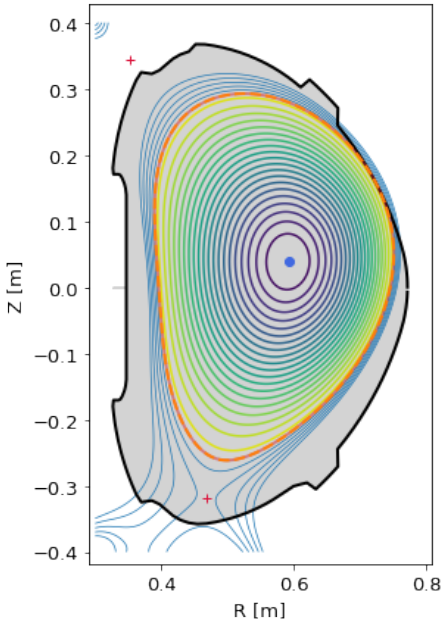

Figure 3.3: Flux surfaces of the IPR coil corrected equilibrium reconstruction with added flux loops and Mirnov coils. The X-point was clearly created but the flux surface passing through it intersects a limiter.

tering temperature measurement to place a constraint on the separatrix position in EFIT++. This analysis and equilibrium reconstruction were provided by M. Šos and M. Komm.

Equilibrium reconstructions using these methods were carried out on COMPASS discharge #17692 at 1120 ms. Figure 3.2 shows the separatrix position plotted in a poloidal cross section of COMPASS chamber. The most glaring outlier is the reconstruction with corrected IPR coil position and flux loop, Mirnov coil measurements. The reconstruction would suggest that the plasma is in a limiter configuration. This does not, however, mean that X-point was not created. Figure 3.3 shows that an X-point exists but the flux surface passing through it intersects a limiter. Divertor measurements (Fig. 3.4) however show that this is obviously not the case. As most of radial transport from the confined plasma happens at the outer midplane, temperatures and heat fluxes at least at the inner strike point would be greatly or completely diminished. Divertor measurements, however, show both strike points with parameters expected for a divertor configuration. It is important to mention that the position of the separatrix when comparing the reconstructions describes slightly different quantities. One represents the last closed flux surface constrained by the limiter, while the other represents the flux surface passing through and constrained by the position of the X-point.

3.3 Validating equilibrium reconstructions based on experimental data alone

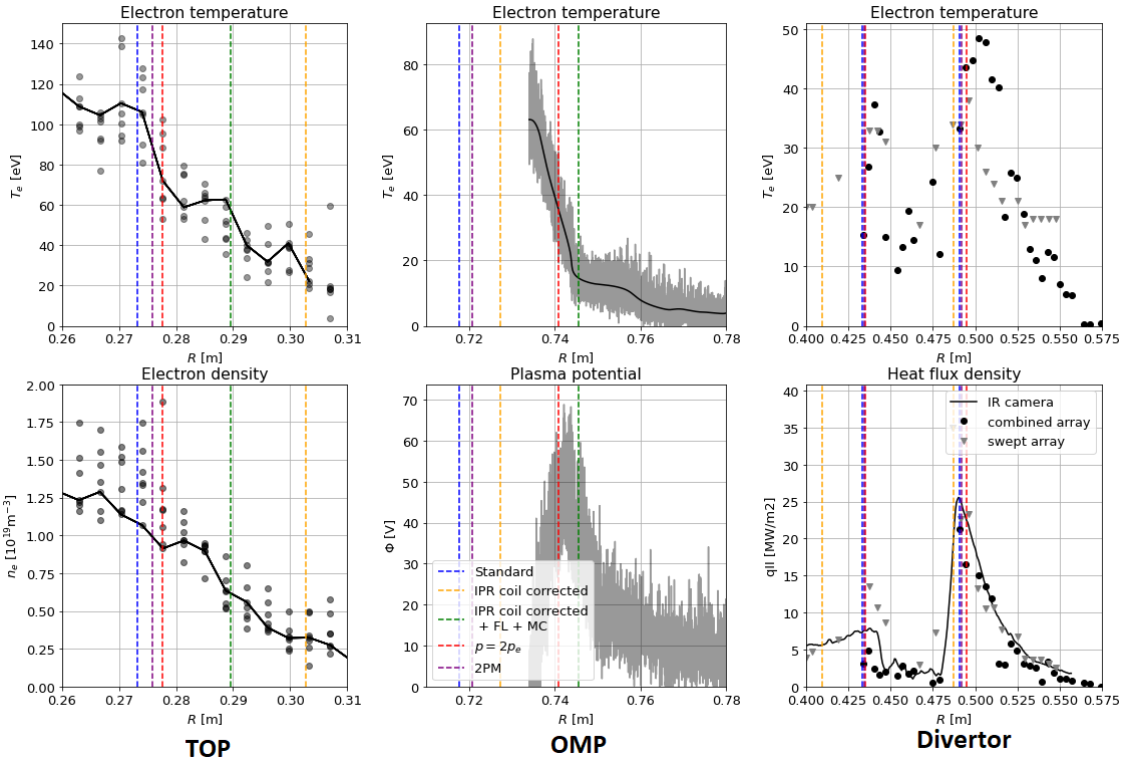

Figure 3.4: Comparison between the diagnostic data and the separatrix position. The separatrix is marked for each equilibrium reconstruction by a vertical line. The colors correspond to the reconstructions in figure 3.2. The left column shows measurements at the plasma top, the middle column shows measurements at the outer midplane and the right column shows divertor measurements.

The equilibrium reconstructions can be compared with experimental data only to make several observation. Figure 3.4 shows key diagnostic measurements at the plasma top, the outer midplane (OMP) and at the divertor compared with the reconstructed separatrix positions. The diagnostic measurements are gathered from a time period before the horizontal reciprocating probe penetrates deep into the plasma. Although the probe starts moving through the SOL at 1100 ms, it reaches the velocity shear layer at approximately 1160 ms. The Thomson scattering, the probe arrays and the infrared camera measurements are thus taken from the time period of 1100-1160 ms. The position of the separatrix in the figure is marked by a vertical line for each equilibrium reconstruction, and the colors correspond to those in figure 3.2. The equilibrium reconstructions were evaluated based on three main criteria.

In the first criterion, one can compare the electron temperature measured at the plasma top and at the OMP for each equilibrium reconstruction. The high parallel transport should equalize upstream electron temperature at the separatrix. Assuming the SOL is sheath-limited, which is presumed to be the case for COMPASS most

of the time, the electron temperature should also be similar at the strike points. The figure, however, shows significant differences. Let us take the IPR coil corrected reconstruction (orange) as an example. At the separatrix at the plasma top, the electron temperature at the separatrix is roughly in the range 20 eV to 50 eV and although data directly at the separatrix at the OMP are not available, we know the electron temperature is 50 to 80 eV further away in the SOL. It is hard to judge which equilibrium reconstruction performs the best in this criterion as only two out of five have separatrix measurements on both upstream locations. Nevertheless, the $p = 2p_e$ reconstruction performs reasonably well.

The second criterion uses the plasma potential maximum measured at the OMP. The maximum suggests that the reciprocating probe has reached the VSL. While it is not known where exactly relative to the separatrix VSL forms, systematic studies at COMPASS have shown that it should be relatively close outside the separatrix. [6] Assuming the separatrix is directly at this maximum, the equilibrium reconstructions can also be evaluated based on the separatrix positions relative to it. The $p = 2p_e$ reconstruction is closest to the potential maximum.

Lastly, in an attached plasma the maximum of heat flux density on the divertor targets should be located at the strike points. In this regard, the equilibrium reconstructions do not show significant differences except for the IPR coil corrected equilibrium reconstruction, where the inner strike point position is clearly incorrect.

The set of assumptions used in these evaluations may not be universally true. Simulations of the SOL can provide evaluations without the assumptions and with greater accuracy. Nevertheless, the $p = 2p_e$ equilibrium reconstruction (red) was chosen for the initial simulations using SOLPS-ITER based on this evaluation. Its separatrix at the OMP is the closest one to the potential maximum and it has a reasonable difference between upstream separatrix temperatures.

3.4 Matching SOLPS-ITER simulations to experimental data

This thesis uses SOLPS-ITER version `3.0.7-41-g0c21b66`. A magnetic equilibrium file and COMPASS chamber geometry were loaded into the `divgeo` program to prepare the simulation geometry. Programs `carre` and `triang` were then used to create the B2.5 and EIRENE meshes respectively (Fig. 3.5). The default initial state was also generated. In all subsequent simulations, the final state of a converged run was used as an initial state in the next simulation. Convergence of the simulation was determined by general steadiness of various plasma parameters such as the OMP separatrix temperature and of the B2.5 equations residuals. The process of achieving a match between the simulation and the experiment was done in an iterative approach by changing free input parameters based on observations in previous simulations. These input parameters include core boundary conditions (deuterium density at the innermost flux surface and the power injected across this flux surface into the simulation domain) and the anomalous transport coefficients $D_\perp$ and $\chi_e = \chi_i$.

Figure 3.5: B2.5 and EIRENE mesh created using the $p = 2p_e$ equilibrium reconstruction.

Uncertainties in the experimental measurements present a certain flexibility in the input parameters.

As was discussed in the previous section, the experimental data show a significant difference in separatrix temperature at the plasma top and at the OMP. Even when taking uncertainties into account, the significant differences make matching the simulation to the experiment difficult. A commonly used approach to fix this is to shift the experimental and simulation data relative to each other to achieve a better agreement. This *separatrix shift* creates additional free parameters to achieving a better model-experiment match.

For an example of a simulation without employing the separatrix shifts, see figure 3.6. Looking at the simulation data, the previously mentioned assumption that electron temperature is equal at the plasma top, and similar at the divertor strike points, appears to hold true in the simulation. The figure shows that attempting to find a better model-experiment match without the separatrix shifts in not feasible. For example, changing boundary conditions or transport coefficients to decrease temperature and provide a better match at the plasma top would result in unrealistic temperature profile at the OMP.

The $p = 2p_e$ equilibrium reconstruction (red) was chosen for the initial simulation based on the evaluation in the previous section. By following the iterative approach a match between the simulation and the experiment was found. At the core boundary, the ion density was set to $n_i = 1.4 \times 10^{19}$ m^{-3}. The power balance was maintained by core boundary energy flux $P_{SOL} = 150$ kW, split equally between ions and electrons. The particle diffusion coefficient was $D_\perp = 0.3$ m^{2}s^{-1} and the thermal diffusion coefficient were $\chi_{i,e} = 1.2$ m^{2}s^{-1}, same for electrons and ions. The only simulated

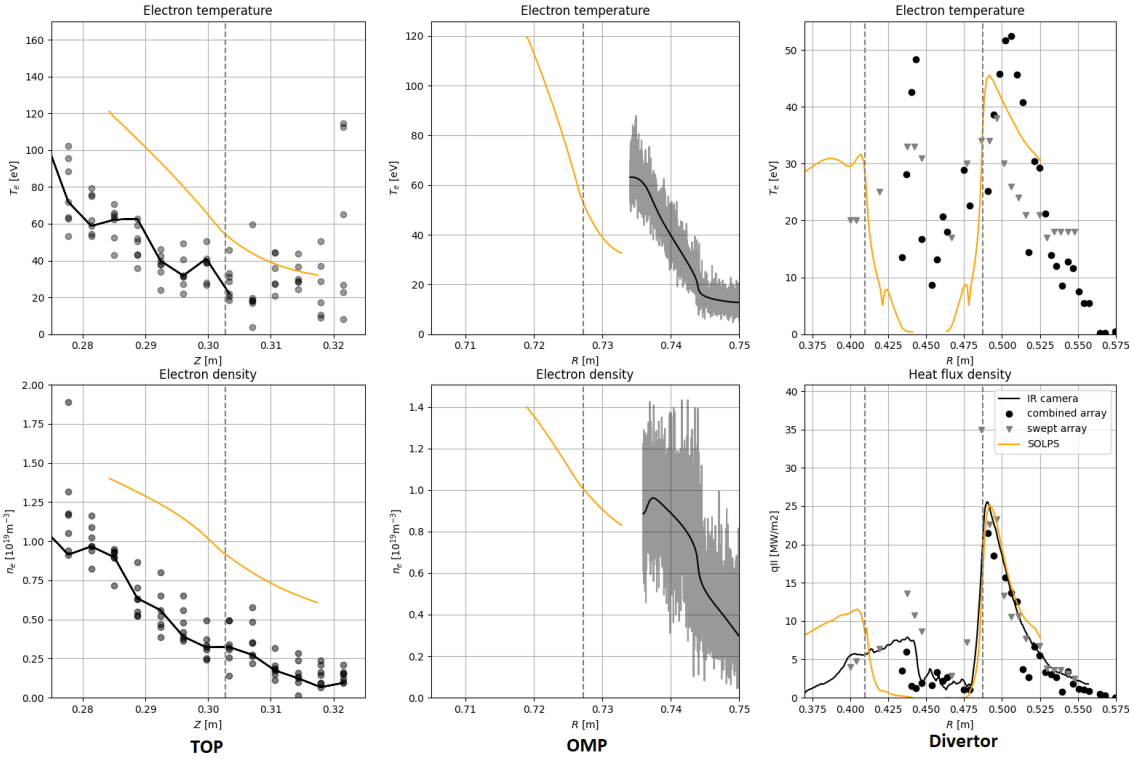

Figure 3.6: Comparison between the diagnostic data and the simulation data using the IPR coil corrected equilibrium. No separatrix shifts were employed.

ion species was deuterium. No impurities were used and graphite target sputtering was turned off. Drifts were also turned off. Although attempts were made to match the simulation to the experiment with only shifting the separatrix at the plasma top, due to the separatrix at the OMP being close to the VSL, this proved to be unfeasible and both corrections had to be used. The separatrix shifts found to provide the best match are $\Delta Z = 4$ mm radially outward at the plasma top (to the right) and $\Delta R = 3$ mm inward at the OMP (to the left). This match is shown in figure 3.7 compared with simulations discussed further.

The equilibrium reconstructions for the next simulations were then selected. The 2PM equilibrium reconstruction was chosen. Its separatrix position is very similar to the standard reconstruction and both are practically interchangeable. However, it performs slightly better when evaluated against the experimental data. Looking at the equilibrium reconstructions comparison 3.2, the biggest outliers seem to be the two reconstructions with corrected IPR coil positions and angles. The equilibrium with added magnetic diagnostic measurements is in a limited configuration and is thus unsuitable for SOLPS-ITER modeling. The IPR corrected equilibrium without the additional magnetic measurements was chosen for another simulation to experiment match. The large difference in the separatrix position compared to the other reconstruction made it a compelling choice for further study. The equilibrium reconstructions were then used to construct their respective meshes and simulation geometry. To study the effect of the mesh on the model-experiment match, the same exact input parameters as in the $p = 2p_e$ simulation (transport coefficients, boundary conditions) were used in the simulations using the other equilibrium re-

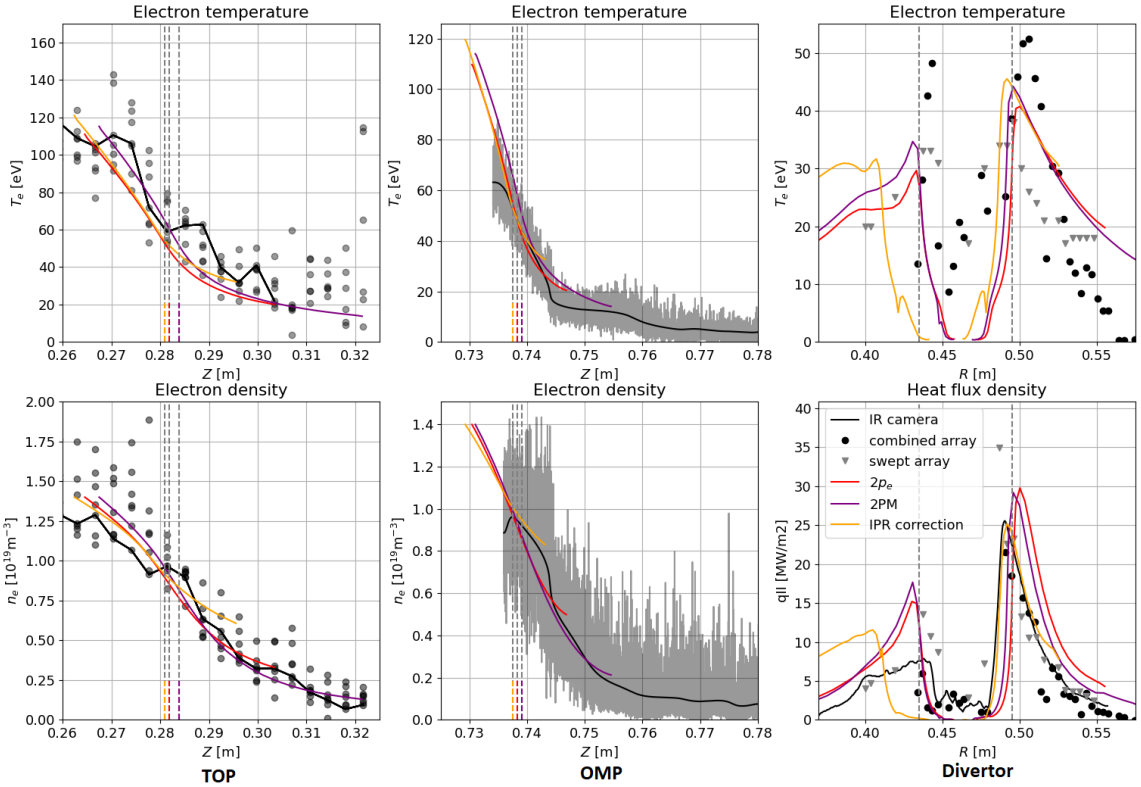

Figure 3.7: Comparison between the diagnostic data and the simulation data. The colors correspond to the reconstructions in figure 3.2. The separatrix position is marked by a vertical line highlighted by the corresponding color. The separatrix shifts used are in table 3.1.

constructions. The only differences are the top and OMP separatrix shifts. Both simulations converged successfully.

As the separatrix position is different in each equilibrium reconstruction, the separatrix shifts providing the best model-experiment match were needed to be found independently, see Tab. 3.1. However, the diagnostic measurement uncertainties allow for considerable flexibility in determining the separatrix shifts, up to several millimeters. Figure 3.7 shows all three equilibrium reconstruction compared with experimental data. The shifted separatrix position for each equilibrium reconstruction is marked by a vertical line. It is evident that despite the simulations being based on equilibrium reconstructions with very different separatrix positions, the corrected separatrix positions all converge to a position a few millimeters from each

reconstruction	ΔR [mm]	ΔZ [mm]	R [mm]	Z [mm]
$p = 2p_e$	-3	4	738	282
2PM	18	8	739	284
IPR corrected	10	-22	738	281

Table 3.1: Optimal separatrix shifts for each used equilibrium reconstruction: at the outer midplane ΔR, at the plasma top ΔZ. The absolute position of the separatrix at the OMP R, at the plasma top Z.

other. Considering the uncertainty in choosing the separatrix shifts, it can be said that optimal separatrix position for each simulation is at the same absolute position.

The left column of the figure 3.7 displays a match between the SOLPS-ITER simulation data and the Thomson scattering measurements. The middle column of the figure shows the horizontal reciprocating probe measurements. The separatrix shifts corrected the disagreement between the separatrix temperature at the plasma top and the OMP. The simulation data on both upstream positions falls within the fluctuation of the diagnostics. The diagnostic measurements show a lower electron temperature in the confined plasma at the OMP. This is due to the cooling effect of the horizontal reciprocating probe. The right column of the figure shows divertor measurements. No shifts were done to the strike point positions at the divertor, as the match between the simulation and the experiment is evident even without them. There is a slight disagreement between heat flux measurements of the combined array, the swept array and the IR camera, creating an uncertainty in the measurements. The peak value of heat flux density falls within this uncertainty. The profile shape also seems to match the experimental data.

It is evident that there are only minor differences between the simulation results. The biggest difference is unsurprisingly at the IPR coil corrected equilibrium reconstruction's inner strike point. The fact that the results are similar and the separatrix is shifted to the same position suggests that a more realistic separatrix position was found. The fact that the transport coefficients and boundary conditions lead to a very similar result on different meshes suggests that they describe the experiment well and the simulations are not over-fitted.

3.5 Plasma-limiter interaction

Analysis of how heat flux moves through simulation boundaries shows that simulations with the $p = 2p_e$ and IPR coil corrected equilibrium reconstructions have a larger portion of their total heat flux moving through the far SOL boundary. Looking back at the equilibria comparison (Fig. 3.2), both equilibrium reconstructions have a small clearance between the separatrix and the LFS poloidal limiter of around 12 mm. In the simulation, this limits the extent of the mesh (Fig. 3.5) allowing for a larger portion of the heat to reach the far SOL boundary where it is lost. In the experiment, this small clearance should result in a portion of the SOL being scraped off by the limiter. As most of the heat flux leaves the core region at the OMP, this effect could be seen at the inner divertor target. The heat flux measurements at the inner target are, however, insufficient to make that determination.

Although the IPR coil corrected equilibrium reconstruction has a low clearance of 12 mm, the simulation mesh is not bounded by the LFS limiter but by a HFS top limiter, unlike the $p = 2p_e$ reconstruction (see Fig. 3.8). In an unpublished study by J. Cavalier at IPP CAS, it has been shown that when the clearance between the separatrix and the LFS limiter is less than 15 mm, the plasma-wall interaction is observable on visible camera data. Both the LFS limiter and the HFS top limiters are within the field of view of a visible light camera, see Fig. 2.1. Figure 3.9 shows the

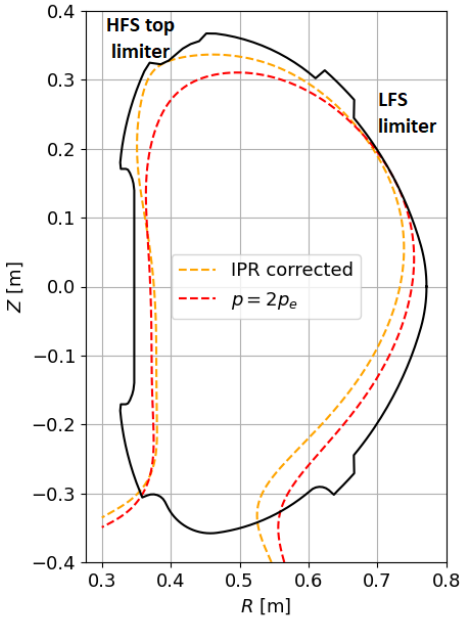

Figure 3.8: The flux surfaces limiting the extent of the mesh for the IPR coil corrected and the $p = 2p_e$ equilibrium reconstruction.

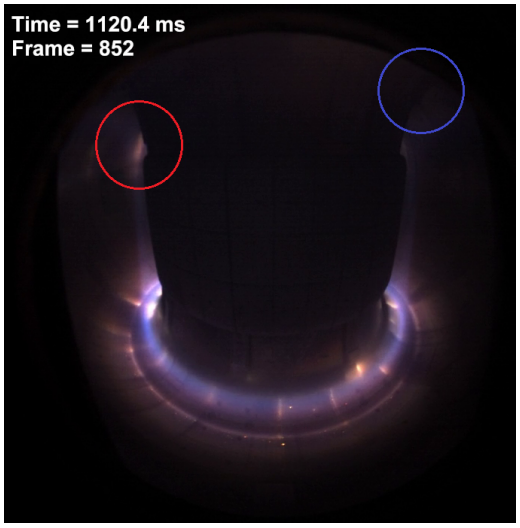

Figure 3.9: Visible light camera showing the LFS limiter (red) and the HFS top limiter (blue).

captured image at the simulated time. The light coming from the LFS limiter can be clearly seen, while the HFS top limiter shows no such interaction. This would suggest that the plasma in the experiment is bounded by the LFS limiter rather than the HFS top limiter. Thus, the IPR coil corrected equilibrium reconstruction is likely inaccurate at the plasma top.

Conclusion

This thesis evaluated different methods of magnetic equilibrium reconstructions of COMPASS tokamak using simulations with SOLPS-ITER edge transport code in discharge #17692. Five variants of the equilibrium reconstruction were performed and compared to experimental measurements. The $p = 2p_e$ equilibrium reconstruction with realistic pressure profile was chosen based on this comparison as the best candidate for further modeling. The simulation based on this equilibrium reconstruction was then matched with the experimental measurements. For an accurate model-experiment match, the separatrix position had to be corrected by shifting the simulation data relative to the experimental data. Three SOLPS-ITER simulations based on three equilibrium reconstruction variants were performed using the same input parameters (anomalous cross-field transport coefficients, boundary conditions) and differing only in separatrix position shifts. The conclusion was that the simulation results were identical within experimental uncertainties, and that the optimal separatrix position lies at the same position in each case. The equilibrium reconstruction requiring the smallest separatrix shifts was the initial $p = 2p_e$ reconstruction with realistic pressure profile.

The simulations results having only minor differences has implications for future SOLPS-ITER modeling. This outcome gives validity to interpretative simulations using inaccurate equilibrium reconstructions. As long as these inaccuracies can be corrected with separatrix shifts by comparison with experimental data and by the iterative approach to matching the simulation, the result should not be significantly altered. At least, this conclusion can be made for the simple SOL and open divertor of tokamak COMPASS. In a more complicated divertor geometry, a small error in separatrix position may constitute the difference between the strike point being on the divertor target and the strike point being on the divertor baffle, which would evidently impact the overall result.

The fact that each simulation was well matched by the separatrix being shifted to the same positions while also resulting in very similar plasma parameters also gives validity to using the separatrix shifts in the first place. This approach is commonly used in SOLPS-ITER modeling simply because without it, the simulation could not be matched accurately to the experiment. Shifting the data up to 18 mm outwards and 3 mm inwards at the outer midplane, 4 mm outwards and 22 mm inwards at the plasma top has no significant effect on the final result and there is no ambiguity in the result.

The separatrix shifts moving the separatrix to the same position is also interesting for

the equilibrium reconstructions. This result would suggest that a better separatrix position was found, at least at the plasma top and the OMP. These values can be used as additional constraints for EFIT, which will result in a SOLPS corrected equilibrium reconstruction. The process of creating a SOLPS simulation for every equilibrium reconstruction, however, is too time-intensive to be used routinely. It can be applied in cases where an accurate reconstruction is particularly important, e.g. a well-diagnosed experiment which provides basis to interpretative modelling using several codes.

This thesis gives a valuable insight into tokamak edge plasma modeling. It shows that the influence of equilibrium reconstruction variants is relatively small and that the separatrix shifts indicate optimal separatrix position. SOLPS-ITER can thus be used to improve magnetic equilibrium accuracy when it is required. The validity of the separatrix shifts confirms it to be a useful tool for interpretative modeling. These results contribute to our ability to perform simulations of tokamak edge plasma and advance our understanding of edge plasma physics for both interpretative simulations and predictive simulations for future fusion reactors such as COMPASS Upgrade and ITER.

Bibliography

[1] J. Wesson. *Tokamaks; 4th ed.* Oxford Univ. Press, 2011.

[2] W. Tang et al. Global simulation of plasma microturbulence at the petascale and beyond (optimizing the gtc code for blue gene/q): Alcf-2 early science program technical report, 05 2013.

[3] Harold Grad and Hanan Rubin. Hydromagnetic equilibria and force-free fields. *Journal of Nuclear Energy*, 7:284–285, 1958.

[4] EFIT. `https://omfit.io/modules/mod_EFIT.html`. Accessed: 2024-05-10.

[5] L.C. Appel et al. Equilibrium reconstruction in the start tokamak. *Nuclear Fusion*, 41(2):169, feb 2001.

[6] K. Jirakova et al. Systematic errors in tokamak magnetic equilibrium reconstruction: a study of EFIT++ at tokamak COMPASS. *Journal of Instrumentation*, 14(11):C11020, nov 2019.

[7] P.C. Stangeby. *The Plasma Boundary of Magnetic Fusion Devices.* Series in Plasma Physics and Fluid Dynamics. Taylor & Francis, 2000.

[8] D. A. D'Ippolito et al. Convective transport by intermittent blob-filaments: Comparison of theory and experiment. *Physics of Plasmas*, 18(6):060501, 06 2011.

[9] K. Jiráková. *Study of edge plasma of tokamak COMPASS and its poloidal variations, Master's thesis.* Czech Technical University in Prague, 2018.

[10] P. Kulhánek. *Vybrané kapitoly z teoretické fyziky.* 01 2020.

[11] S. I. Braginskii. Reviews of plasma physics. In *Reviews of Plasma Physics*, 1965.

[12] M. G. Haines. 'transport processes in plasmas' vol. 1: Classical transport; vol. 2: Neoclassical transport, r. balescu, north-holland press, 1988. *Journal of Plasma Physics*, 43(3):483–485, 1990.

[13] V. Zhdanov. *Transport Processes in Multicomponent Plasma.* 04 2002.

[14] S. Wiesen et al. The new SOLPS-ITER code package. *Journal of Nuclear Materials*, 463:480–484, 2015. PLASMA-SURFACE INTERACTIONS 21.

[15] D. P. Coster et al. *SOLPS manual, version 3.0.7-41-g0c21b66*. ITER.

[16] M. Hron et al. Overview of the compass results. *Nuclear Fusion*, 10 2021.

[17] Tokamak COMPASS. `https://www.ipp.cas.cz/vedecka_struktura_ufp/tokamak/COMPASS/`. Accessed: 2024-05-10.

[18] K. Hromasová et al. SOLPS-ITER simulations of the COMPASS tokamak. In *47th EPS Conference on Plasma Physics 2021*, 2021.

[19] P. Bílková et al. Design of new thomson scattering diagnostic system on COMPASS tokamak. *Nuclear Instruments and Methods in Physics Research Section A: Accelerators, Spectrometers, Detectors and Associated Equipment*, 623(2):656–659, 2010. 1rs International Conference on Frontiers in Diagnostics Technologies.

[20] V. Weinzettl et al. Overview of the COMPASS diagnostics. *Fusion Engineering and Design*, 86(6):1227–1231, 2011. Proceedings of the 26th Symposium of Fusion Technology (SOFT-26).

[21] J. Adamek et al. Profile measurements of the electron temperature on the ASDEX Upgrade, COMPASS, and ISTTOK tokamak using Thomson scattering, triple, and ball-pen probes. *Review of Scientific Instruments*, 87(4):043510, 04 2016.

[22] Divertor probes in compass. `https://www.ipp.cas.cz/vedecka_struktura_ufp/tokamak/COMPASS/diagnostics/diagnostiky-sondami/divertorove-sondy.html`. Accessed: 2024-05-10.

[23] J. Adamek et al. Electron temperature and heat load measurements in the COMPASS divertor using the new system of probes. *Nuclear Fusion*, 57(11):116017, aug 2017.

[24] J. Hečko et al. Experimental evidence of very short power decay lengths in h-mode discharges in the COMPASS tokamak. *Plasma Physics and Controlled Fusion*, 66(1):015013, dec 2023.

[25] M. Komm et al. On the applicability of three and four parameter fits for analysis of swept embedded langmuir probes in magnetised plasma. *Nuclear Fusion*, 62(9):096021, aug 2022.

[26] O. Vondracek et al. Fast infrared thermography on the COMPASS tokamak. *Fusion Engineering and Design*, 123:764–767, 2017. Proceedings of the 29th Symposium on Fusion Technology (SOFT-29) Prague, Czech Republic, September 5-9, 2016.

[27] O. Kovanda et al. Dependence of reconstructed equilibria on input data sets using EFIT on COMPASS and comparison with experimental observations. 2019.